JOURNAL OF PROPULSION AND POWER
Vol. 21, No. 1, January–February 2005

Performance Analysis of Microthrusters Based on Coupled Thermal-Fluid Modeling and Simulation

A. A. Alexeenko,* D. A. Levin,† D. A. Fedosov,* and S. F. Gimelshein‡
Pennsylvania State University, University Park, Pennsylvania 16802
and
R. J. Collins§
University of Minnesota, Minneapolis, Minnesota 55455

Gas flow and performance characteristics of a high-temperature micro-electronically machined systems (MEMS)-based thruster are studied using a coupled thermal-fluid analysis. The material thermal response governed by the transient-heat-conduction equation is obtained by the finite element method. The low–Reynolds number gas flow in the microthruster is modeled by the direct simulation Monte Carlo approach. The effects of Reynolds number, thermal boundary conditions, and micronozzle height are considered in detail. The predicted thrust and mass-discharge coefficient of the three-dimensional microthruster under different flow conditions decrease with time as the viscous losses increase for higher wall temperatures.

Nomenclature

a	=	speed of sound
c_p	=	specific heat at constant pressure
h	=	height of nozzle
h	=	heat-conduction coefficient
k	=	thermal conductivity
$\dot{m}$	=	mass flow rate
N	=	number of particles
$\mathcal{P}$	=	inlet-to-outlet pressure ratio
p	=	pressure
q_a	=	conductive heat flux
q_c	=	convective heat flux
q_r	=	radiative heat flux
R	=	gas constant
Re	=	Reynolds number with respect to the throat dimension
T	=	temperature
u	=	X component of velocity
v	=	Y component of velocity
Δt	=	computational time step
Δx	=	cell size
ρ	=	density
σ	=	accommodation coefficient
τ_λ	=	mean time between collisions
τ_{res}	=	mean residence time in a cell
Ω	=	domain of the finite element method (FEM) solution

Subscripts

o	=	stagnation
w	=	wall
λ	=	linear size equal to local mean free path
∞	=	freestream

Presented as Paper 4717-2003 at the Coupled Thermal-Fluid Modeling of Micronozzles for Performance Analysis, Huntsville, AL, 20–23 July 2003; received 21 September 2003; revision received 4 June 2004; accepted for publication 18 June 2004.

*Graduate Student, Department of Aerospace Engineering. Member AIAA.
†Associate Professor, Department of Aerospace Engineering. Senior Member AIAA.
‡Senior Research Associate, Department of Aerospace Engineering. Member AIAA.
§Professor Emeritus, Department of Electrical Engineering.

I. Introduction

DEVELOPMENTS in MEMS-based micropropulsion technology are being considered for application in space propulsion, particularly by NASA for spacecraft formation flying. Formation flying of miniature spacecraft will demand a wide range of propulsion maneuvers such as orbit raising, drag makeup, stationkeeping, and deorbit. Typically impulse bits on the order of mN s will be required for such microspacecraft missions.

New propulsion systems are needed that are able to deliver precise impulse bits while meeting strict mass, size, and power-usage limitations. The advantages of MEMS-based propulsion devices for such missions include lightweight materials, high degree of integration between different components, ability to provide versatile thrust levels, and, finally, the potential to batch manufacture such devices. A MEMS-based propulsion system might consist of arrays of microrocket thrusters on a silicon chip with electronic circuitry that controls the firing. Cold gas,[1,2] catalytic decomposition,[3] vaporizing liquid,[4] and mono and bipropellant[5] thrusters are among the various micropropulsion concepts currently being evaluated.

The flowfield of the typical low–Reynolds number micronozzle device cannot be calculated using conventional computational fluid dynamics techniques because the continuum assumption is not applicable throughout the flow.[6] The Knudsen number, based on the MEMS nozzle throat diameter, is on the order of 10^{-3} and grows several orders of magnitude at the nozzle exit. In this flow regime, the direct simulation Monte Carlo (DSMC) method, a kinetic approach, provides the most accurate numerical flowfield results.

Because of the reduced physical size of microthrusters, surface effects such as friction and heat transfer can dominate the gas flow in microdevices and, in a high-temperature microthruster, may necessitate the cooling of its structure. The concept of a micromachined bipropellant rocket engine with regeneratively cooled walls was introduced in Ref. 5. In that work, it was emphasized that the heat-flux and heat-load limits are two major physical-design constraints for such micropropulsion devices.

The nozzle wall temperature and heat fluxes are major factors that influence the gaseous flow dynamics and thruster performance, yet the temporal variation of the thruster temperature is often an unknown in the system design. The burn time of the thruster is an important design parameter that determines the impulse bit that will be available for spacecraft propulsion maneuver. Yet the heating of the microthruster structure by heat transfer between the

high-temperature supersonic flow in the nozzle and thruster walls imposes time limits on its operation.

To expand micropropulsion-system design capabilities, a general method for modeling coupled, time-dependent fluid and thermal behavior in microcombustion devices was developed.[7] In that work, a coupled fluid and thermal model was applied for the first time to high-temperature gas flow in a MEMS device. The developed computational tool allows the accurate computation of wall heat fluxes, temporal variation of the gas flow, and other system parameters without having to specify the unknown wall temperature. The nozzle material thermal response can be expected to have an impact on micronozzle integral quantities such as thrust, specific impulse efficiency, and system specifications such as the maximum operational burn time. The model and computational approach were applied to two- and three-dimensional models of a prototype micropropulsion system being designed and tested at NASA Glenn Research Center[8–10] for $Re = 35$ and 175, corresponding to chamber pressures of 0.1 and 0.5 atm. Two limits of the true thermal environment were considered. The first thermal boundary condition was that of a thermally insulated condition; the convective and conductive heat fluxes were assumed to be zero. The second thermal boundary condition corresponded to that of nozzle actively cooled by a liquid flow at 300 K over the outer surface of the thruster.

A number of significant conclusions may be drawn from that work.[7] There exists a major difference between the gas flowfields inside the three- and two-dimensional models of the microthruster, due to the impact of the sidewall boundary layer present only in the three-dimensional case. The predicted thrust and mass discharge coefficients of both the two- and three-dimensional micronozzles decrease in time as viscous losses increase for higher wall and gas temperatures. The decrease in thrust and mass discharge coefficient as a function of time is greater for the three-dimensional than for the corresponding (thermal boundary condition) two-dimensional cases, again due to the presence of the third surface viscous losses.

Reference 7 also introduced a number of new issues regarding the modeling and simulation of coupled high-temperature micronozzle flows and performance. It is the purpose of this paper to address these important numerical and operational issues. First, let us consider the important issue of numerical accuracy. As mentioned, the gas flowfield is simulated using the DSMC particle method. The correct use of this technique requires one to ensure that the simulations are converged with respect to the number of particles in the computational domain, number of particles per cell, correct choice of time step, and adequate spatial resolution (or number of cells). When multiple flow solutions have been examined with respect to variations of these numerical parameters, the accuracy of the flow simulation and hence nozzle operating parameters may be assessed. In performing the calculations discussed in Ref. 7, it was found that flowfield solutions obtained with the stagnation pressure of 0.1 atm for both two- and three-dimensional nozzle models and with the stagnation pressure of 0.5 atm for the two-dimensional nozzle were rigorously converged with respect to the aforementioned numerical parameters.

However, this was not the situation for the second stagnation pressure considered, that of 0.5 atm for the three-dimensional nozzle. A detailed numerical study fixing the thermal boundary condition (and wall temperature) will be presented for the three-dimensional, 0.5-atm pressure case and the implications for modeling of such micronozzle systems with DSMC will be discussed.

Second, the work of Ref. 7 demonstrated that for the lower–Reynolds number condition, stagnation pressure of 0.1 atm, the viscous losses were greatest (particularly for the three-dimensional nozzle). Hence in this work we consider a nozzle optimization study for the lower stagnation pressure and the adiabatic thermal (the more stressing) boundary condition. The flow and thermal simulations will be fully coupled, as in earlier work, and an improved material thermal model including radiation losses is also used.

The outline of the paper is as follows. In Secs. II and III the micronozzle geometry, flow conditions, and numerical approaches are discussed. In Sec. IV the thermal conditions are reviewed. In Sec. V the following results are presented. As a measure of macroparameter convergence a study of the gas temperature and streamwise velocity is presented. Comparisons of the three-dimensional transient heat calculations at both stagnation pressures for the three-dimensional micronozzle considered in Ref. 7 are presented to provide the reader with a basis for comparison for the second new aspect of this work, the effects of the Reynolds number. Then a comparison of the flowfields and performance values for a stagnation pressure of 0.1 atm and adiabatic thermal boundary condition is given for a new nozzle shape of twice the height (designated as $2h$) of the original three-dimensional nozzle shape, the original three-dimensional nozzle shape ($1h$), and the two-dimensional nozzle shape ($h = \infty$) of Ref. 7.

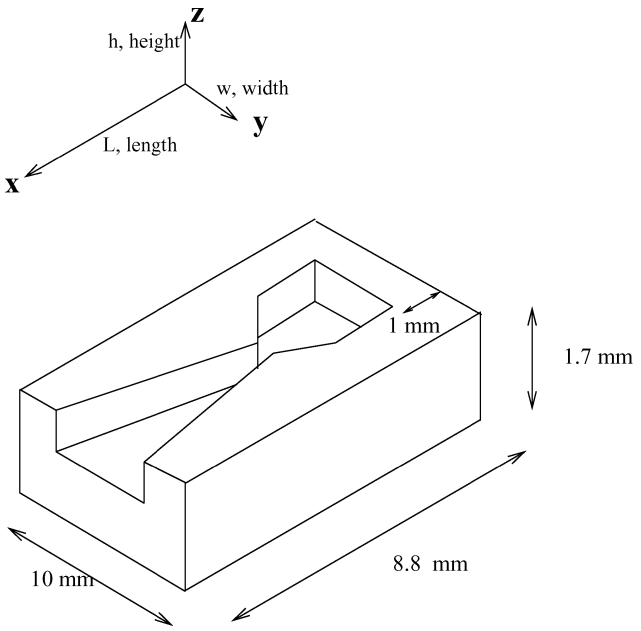

Fig. 1 Schematic of a half-section of the microthruster.

II. Micronozzle Geometry and Flow Conditions

The geometric configuration of the micronozzle studied in this work corresponds to the microthruster design proposed by NASA Glenn researchers. A schematic of the single microthruster modeled here and the axis notations used henceforth are shown in Fig. 1. The dimensions of the outer surfaces of the thruster are as shown in the figure. The micronozzle has throat width 300 μm, height 600 μm (a case with height 1200 μm was also calculated), and length 250 μm. The converging part of the nozzle has a half-angle of 30 deg and an inlet-to-throat-area ratio of 10. The expansion half-angle of the diverging part is equal to 15 deg with an exit-to-throat-area ratio of 5. Because of the computationally intensive nature of the calculations, two- and three-dimensional versions of this nozzle was modeled. The two-dimensional nozzle corresponds to a cut of the three-dimensional geometry parallel to the x–y plane with infinite height, h. In the discussion of the three-dimensional results, the term "sidewall" will be used. This refers to the x–y planes at $z = 0$ and $z = h$ of the three-dimensional nozzle.

The high-temperature flow inside the proposed microthruster will be generated by laser-ignited solid monopropellant decomposition. In the present modeling study, the flow of molecular nitrogen, one of the major components of the decomposition products, was simulated at stagnation pressures of 0.1 and 0.5 atm and a stagnation temperature of 2000 K. Reynolds numbers based on the throat width of 300 μm are equal to 35 and 175 for these two pressures, respectively.

III. Numerical Method

The proposed computational approach is based on the solution of the transient conductive heat-transfer problem coupled with the DSMC solution of the gas flow inside a thruster. The coupling between the material thermal response and fluid flow is carried out

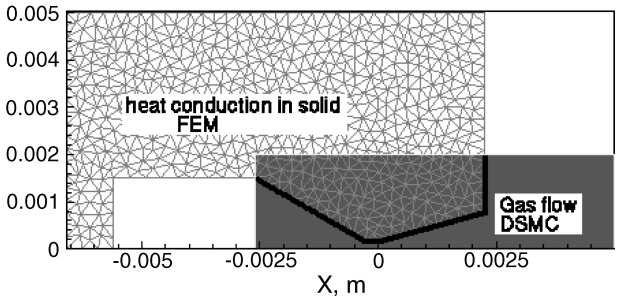

Fig. 2 Computational mesh for two-dimensional coupled calculations.

using the DSMC-calculated heat fluxes as the boundary condition in the heat-conduction problem at the gas–solid interface. The wall temperature calculated in the heat-transfer simulation is in turn applied in the flow simulation.

A. Finite Element Solution

The thermal response of the solid structure is governed by the heat-transfer equation:

$$\frac{\partial(\rho c_p T)}{\partial t} = \nabla \cdot (k \nabla T) \qquad \text{on} \qquad \Omega \tag{1}$$

The boundary conditions for the problem are

$$T|_{\Gamma_1} = T_1, \qquad k\frac{\partial T}{\partial n}\bigg|_{\Gamma_2} = q_a + q_c + q_r$$

where T_1 and T_2 are prescribed temperatures, $\Gamma_1 \cup \Gamma_2 = \partial\Omega$ is the boundary of the domain, and n is the unit vector normal to the boundary.

The numerical solution to the heat-conduction problem can be obtained by the finite element method,[11] which is especially suitable for problems involving complex geometries. In this work, triangular and tetrahedral elements with linear interpolation functions have been used in the finite element solution for the two- and three-dimensional models of the micronozzle, respectively. The details of the finite-element formulation are given in Ref. 7. The unstructured grids were constructed using the GRIDGEN code.[12] Figure 2 shows the triangular grid for two-dimensional microthruster configuration. The mesh has 643 nodes and 1174 triangular elements. The three-dimensional mesh for the microthruster shown in Fig. 1 has 1627 nodes and 7291 tetrahedral elements.

The time integration in the transient heat-conduction calculations is carried out using a first-order purely implicit scheme. The solution of the system of linear algebraic equations resulting from the finite element formulation is obtained by a lower/upper triangular decomposition.

B. DSMC Method

The solution for the gas flow inside the microthruster is obtained by the DSMC method. The DSMC method is a statistical approach to solution of the Boltzmann equation, the governing equation of the rarefied flows. The DSMC method, initially proposed by G. A. Bird in the early 1960s, has become the most powerful and accurate method of numerical modeling of complex rarefied gas flows.[13] The fundamental principle of the DSMC method is the splitting of the dynamics of molecular motion during a time step Δt into two sequential stages: free flight of molecules and intermolecular binary collisions. The DSMC method is non stationary in nature, but can be used to solve stationary problems as well.

Implementation of the DSMC method usually implies the discretization of the flow domain into a grid of cells. The size of computational cells should be sufficiently small so that the change in gas dynamic properties across each cell is small. In each cell, the Knudsen number based on the cell size should be larger than 1. When the cell size in a simulation is too large, macroscopic gradients are typically underpredicted and the solution corresponds to an artificially larger Knudsen number. The time step in the simulation is usually selected so that $\Delta t = \min(\tau_\lambda, \tau_{\text{res}})$, and so that the molecules do not cross more than one cell during a time step. At each time step, the boundary conditions of the flow problem are modeled through particle injection at the domain boundaries and collisions with solid surfaces. After steady flow is reached, sampling of macroparameters within each cell is performed for a time period long enough to minimize statistical scatter.

The parallel DSMC code SMILE[14] is used in these calculations. The VHS model was assumed for the intermolecular collisions, and the Larsen–Borgnakke model was used for energy transfer between translational and internal modes. The Maxwell model with full energy and momentum accommodation was taken for the gas–surface interaction. The total energy flux normal to the surface obtained in SMILE was used in the heat-transfer calculations as the boundary condition, q_a, at the gas–solid interface.

C. Coupling Implementation

In the approach considered here, the coupling between the material thermal response and fluid flow is carried out using the DSMC-calculated heat fluxes as the boundary condition in the heat-conduction problem at the gas–solid interface. The wall temperature calculated in the heat-transfer simulation is in turn applied in the gas-flow simulation.

Let us first estimate the characteristic time scales involved in the transient-heat-transfer problem in a microthruster. The first time scale is associated with the gas flow in the micronozzle, τ_g. This time scale is equal to the residence time of a gas molecule in the nozzle, or $\tau_g = L_s/u_s$, where L_s is the characteristic length scale and u_s is the velocity scale. The second time scale in the coupled-heat-transfer problem is the time constant for the heat transfer in the solid material, τ_s. The time scale τ_s can be estimated using the lumped-capacitance method[15] because the Biot number for microscale devices is small. Using the lumped-capacitance method, $\tau_s = \rho_s L_s c_{p,s}/h_g$, where ρ_s and $c_{p,s}$ are solid density and specific heat at constant pressure, and h_g is the gas convective-heat-transfer coefficient. For example, for $L_s = 100\ \mu$m, $h_g = 10\ \text{W/m}^2 \cdot \text{K}$, and density and specific heat of silicon, $\tau_s \approx 10^{-2}$ s. If the gas is, say, nitrogen at 2000 K, then $\tau_g \approx 10^{-7}$ s. Thus, for a typical microthruster the time scale of the gas flow is much smaller than that for heat conduction in the solid material. A steady-state solution for the gas flow is obtained with the DSMC method, and the DSMC results are then used to update the wall-temperature boundary conditions in the finite element heat-transfer calculations. The updates are performed when the temperature at the gas–solid interface obtained in the heat-transfer solutions changes by several percent.

IV. Thermal Conditions

Two conditions at the external boundary of the microthruster have been studied: (1) zero heat flux (thermally insulated conditions, $q_a = q_c = 0$), designated as no heat removal, and (2) convective heat flux $q_c = h(T - T_\infty)$, $q_a = 0$, designated as cooling. The latter corresponds to the situation where the microthruster wall is actively cooled by a liquid flow with a heat-conduction coefficient $h = 10^3\ \text{W/m}^2 \cdot \text{K}$ and a freestream temperature of 300 K. Such a heat-conduction coefficient is typical for laminar water-flow cooling in microchannels.[16] The liquid-flow active cooling was modeled by assuming that it is used along the perimeter of the rectangular material shape. The thermal properties of the silicon nozzle material were assumed to be constant at $k = 1.412\ \text{W/cm} \cdot \text{K}$, $c_p = 0.7\ \text{J/kg} \cdot \text{K}$, and $\rho = 2.33\ \text{g/cm}^3$. The microthruster material temperatures are limited by the melting temperature of silicon, which is sufficiently low so that radiative heat fluxes were assumed to be negligible ($q_r = 0$). To check this assumption, heat-transfer calculations with radiative cooling of the outer thruster surface to an atmospheric temperature of 300 K and an emissivity of 0.5 were also performed. Comparison of the heat-transfer calculations for $p_0 = 0.5$ atm without convective cooling and with and without radiation heat flux showed only negligible (<10 K) differences in the predicted material temperature.

V. Simulation Results

In this section, results of the numerical simulation using DSMC for the gas flow and finite element methods for the heat transfer in a three-dimensional microthruster under different flow conditions are presented. The cases that are considered here are summarized in Table 1. The simulation in each case involved transient heat-transfer calculations coupled to DSMC solutions for the gas flow inside the nozzle. The transient calculations are needed to establish the variation of the wall temperature with time and the operational time limit of the microthruster. The maximum operational time is the time it takes for the material temperature to reach a value close to the melting temperature, where the structural integrity of the devices may be compromised. For each considered case the flow structure inside the micronozzle was analyzed and performance characteristics such as mass discharge and thrust were calculated as a function of time.

A. Numerical Accuracy

The numerical accuracy of the DSMC solution primarily depends on three main parameters: the cell size Δx, the time step Δt, and the number of particles N_λ in a volume with linear size equal to the local mean free path.[17] In the DSMC algorithm, the cell size has to be less than the local mean free path and the time step should be less than the average time between collisions and a residence time in a cell. An even more strict requirement is that the number of simulated particles has to be large enough to ensure that the statistical correlations between particles are insignificant. All three requirements were satisfied in the calculations for $p_0 = 0.1$ atm, where the linear size of a background cell was taken as 20 μm with four partition levels of grid adaptation, a time step of 1.8×10^{-9} s, and a total of about 2.8 million simulated particles.

For the higher stagnation pressure of 0.5 atm, the DSMC method requirements for cell size, time step, and number of particles are harder to satisfy rigorously. Therefore, to establish the accuracy of the results, a convergence study with respect to time step, number of particles, and cell size was performed. Calculations obtained with different time steps showed that the results do not change for $\Delta t = 1, 2, 4 \times 10^{-9}$ s. The results of additional calculations with the different total numbers of particles of 15 and 30 million and collision cells of 3 and 5 million are shown in Figs. 3 and 4. The temperature

Table 1 Summary of cases considered

Case	p_0, atm	h, μm	Thermal condition
1	0.1	600	No heat removal
2	0.1	600	Cooling
3	0.1	1200	No heat removal
4	0.5	600	No heat removal
5	0.5	600	Cooling

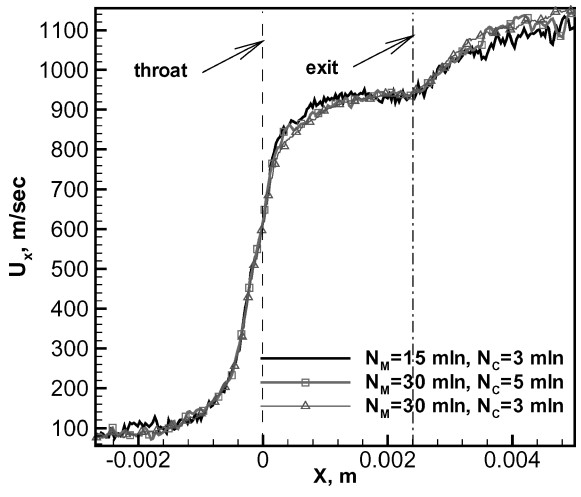

Fig. 3 X component of velocity profile along X axis for case 1.

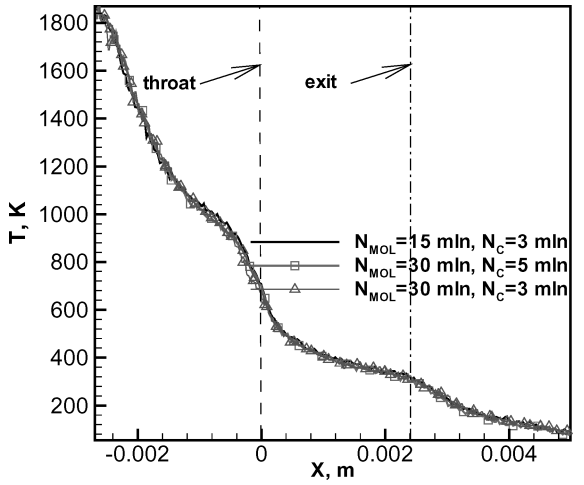

Fig. 4 Translational temperature profile along X axis for case 1.

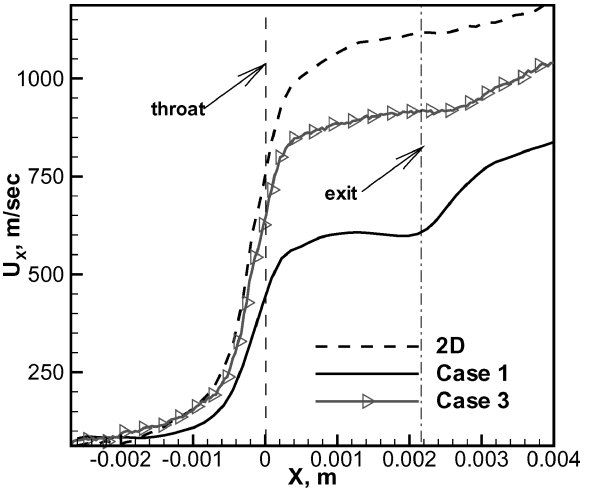

Fig. 5 X component of velocity profile along X axis for two- and three-dimensional simulations.

and X component of velocity inside the micronozzle ($t = 0$ s, initial thermal conditions) are in satisfactory agreement and the maximum difference among the three solutions is less than 3%. Therefore the ratio of real to simulated particles and the grid adaptation level in all $p_0 = 0.5$ atm cases presented in this work were taken to be the same as in the 15-million-particle and 3-million-cell case.

B. Three-Dimensional Geometry Effects

The influence of the geometric shape of the microthruster, in particular its height, on the flow structure and thermal material response can be studied by comparison of cases 1 and 3 and a corresponding two-dimensional case (Ref. 7).

The comparison between the X component of velocity profiles in case 1 ($h = 600$ μm), case 3 ($h = 1200$ μm), and a two-dimensional case that corresponds to infinite height h is shown in Fig. 5. All three cases are for an initial wall temperature of 300 K ($t = 0$). Figure 5 shows that the height of the microthruster has a significant effect on the gas expansion inside the micronozzle. In particular, the X-velocity at the exit for the lowest height is about 55% of the velocity in the corresponding two-dimensional case. The nozzle efficiency increases by doubling the height because the velocity at the exit is 82% of the velocity in the two-dimensional case.

The difference in the thermal responses of the material for microthrusters with different heights is illustrated in Figs. 6 and 7, where the temperature field in the $Z = 0$ plane is plotted for cases 1 and 3, respectively. As one can see, the thruster material temperature reaches 1200 K in about 8 s in case 3, compared to 13 s in case 1. This is due to the larger area of the interface between the material and

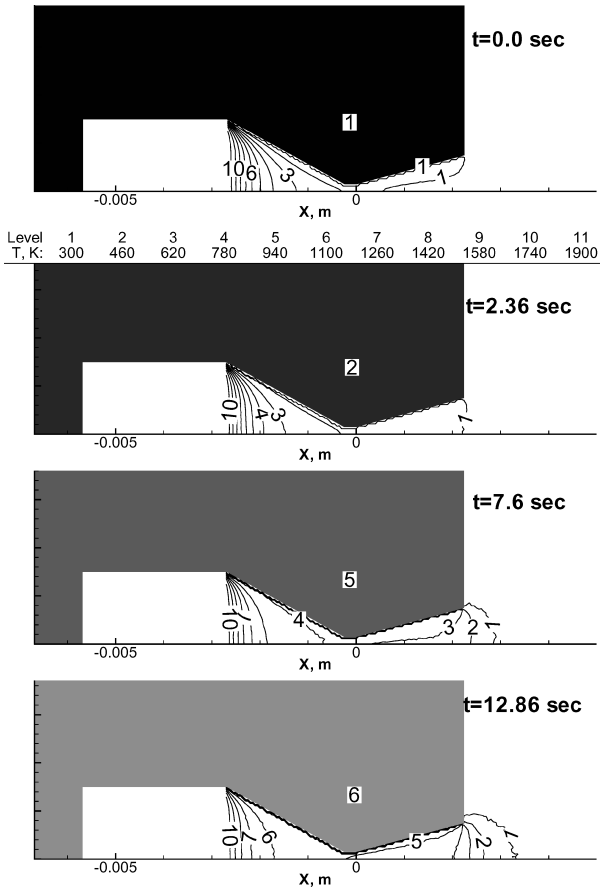

Fig. 6 Temperature field for case 1 in $Z = 0$ plane.

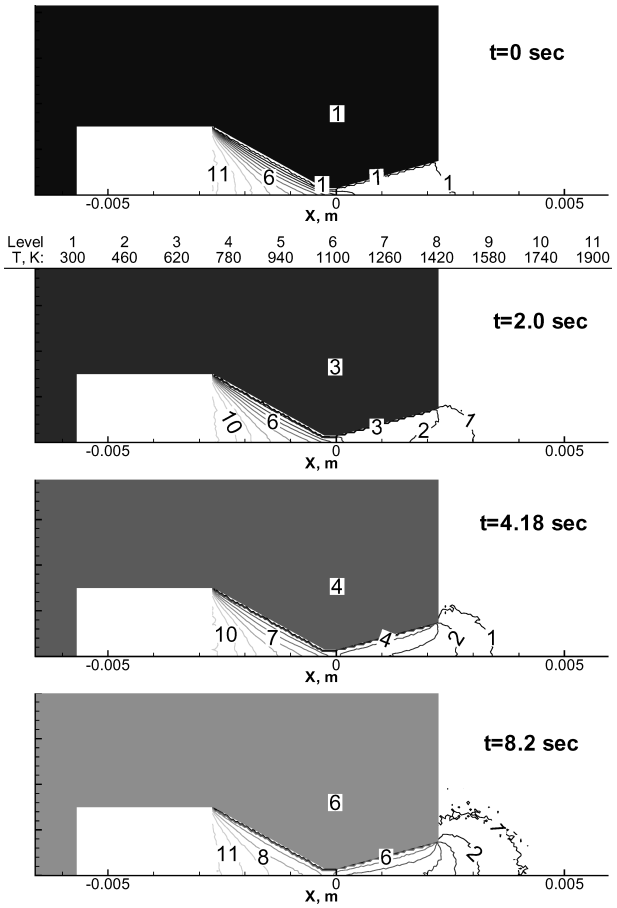

Fig. 7 Temperature field for case 3 in $Z = 0$ plane.

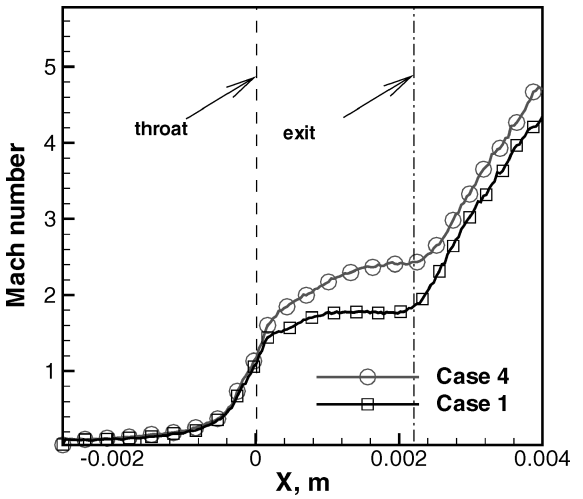

Fig. 8 Mach number profile along X axis for cases 1 and 4.

high-temperature gas flow and a smaller overall volume of material in case 3.

C. Reynolds Number Effects

Let us now consider the effects of the Reynolds number on the flow structure and thermal behavior of the micronozzle. Two nominal Reynolds number cases defined by conditions at the throat are considered, $Re = 35$ and 175, which correspond to stagnation pressures of 0.1 atm (case 1) and 0.5 atm (case 4), respectively.

For the lower pressure case, the gas expansion inside the nozzle is hindered by a thicker boundary layer. Figure 8 shows the Mach number profile along X axis for cases 1 and 4 at $t = 0$ ($T_w = 300$ K). The Mach number in the diverging portion of the micronozzle is significantly less for case 1 than for case 4 and the value of the Mach number at the exit is about 1.9 and 2.4 for the two stagnation pressures 0.1 and 0.5 atm, respectively.

The temperature fields for cases 1 and 4 are plotted in Figs. 6 and 9, respectively. The principal difference between the flows for the two Reynolds number cases is due to the change in the heat flux from the gas to the surface. The heat flux in case 4 is higher by a factor of about 2.6 than in case 1. This causes a larger change of temperature inside the solid material (about 30 K), which is still small compared to the temperature variation in the gas flow. The higher heat flux in case 4 results in a shorter time that it takes the material to reach the melting temperature for case 1. It is about 6 s for case 4 (compared to 14 s for case 1).

D. Effects of Cooling

The effects of cooling applied on the microthruster outer surface can be illustrated by comparison of the calculations for cases 1 and 2 and cases 4 and 5. Figures 6 and 10 show the temperature fields in the $Z = 0$ plane for cases 1 and 2, respectively. As one can see, the temperature inside the microthruster material increases with time for both cases, but by cooling the outer surface of the thruster in case 2, it is possible to sustain the thruster material temperature at a level which is lower than the melting temperature. Similar influence of the applied cooling is observed in cases 4 and 5 (Figs. 9 and 11). The material temperature reaches a value of 1,200 K in about 13 s for case 1 (see Fig. 6) and in about 3 s for case 4 (Fig. 9). But in the cases with applied cooling the calculated steady-state material temperature is about 450 and 650 K in cases 2 and 5, respectively.

Hence, the cooling allows for a longer thruster burn time. For both stagnation pressures the cooling results in higher mass-flow rate and thrust as a function of time (Table 2).

E. Microthruster Performance

Let us now consider the temporal variation of the microthruster performance for the three-dimensional case. Calculated performance parameters of the three-dimensional microthruster are listed

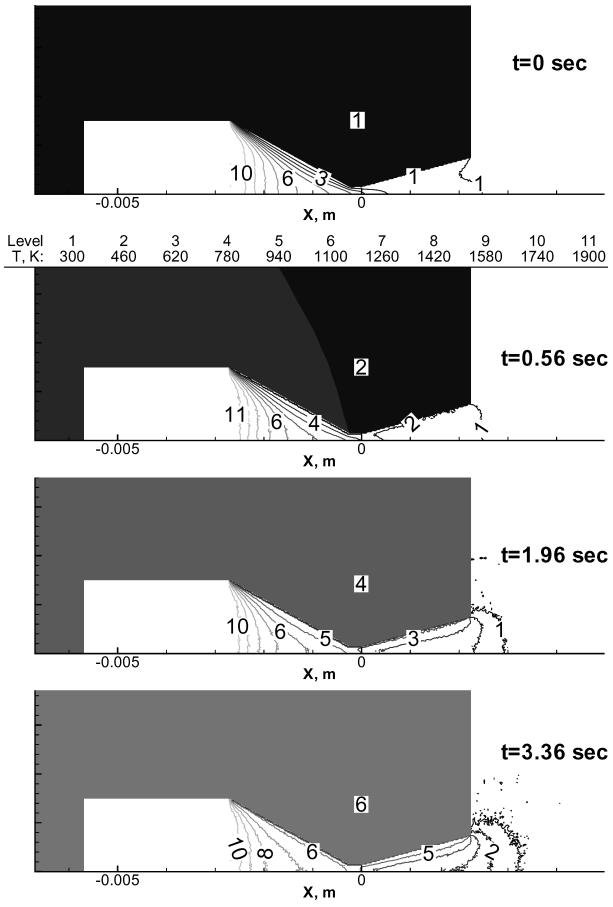

Fig. 9 Temperature field for case 4 in $Z = 0$ plane.

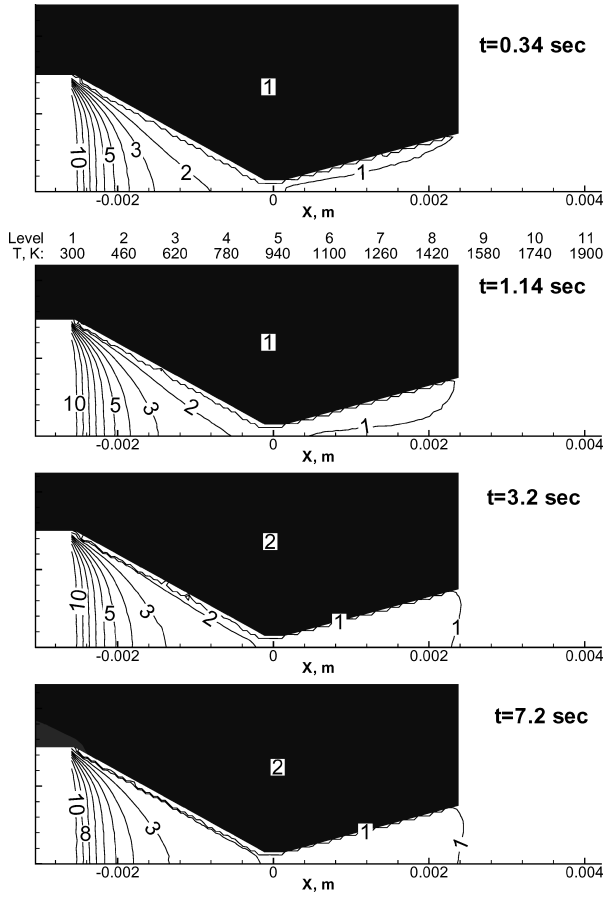

Fig. 10 Temperature field for case 2 in $Z = 0$ plane.

Table 2 Calculated performance

t, s	T_w, K	c_d, %	F, mN
	Case 1		
0	300	0.87	1.44
2.4	500	0.64	1.33
7.6	870	0.48	1.27
12.9	1160	0.41	1.24
	Case 2		
0.34	340	0.87	1.41
1.15	390	0.84	1.38
3.2	440	0.80	1.33
	Case 3		
0	300	0.88	3.49
2.0	530	0.75	3.34
4.18	860	0.66	3.27
8.2	1170	0.57	3.22
	Case 4		
0	300	0.93	9.32
1.96	800	0.75	9.04
3.36	1080	0.68	8.99
	Case 5		
0.64	480	0.88	9.22
1.14	530	0.84	9.12
4.16	650	0.81	9.02

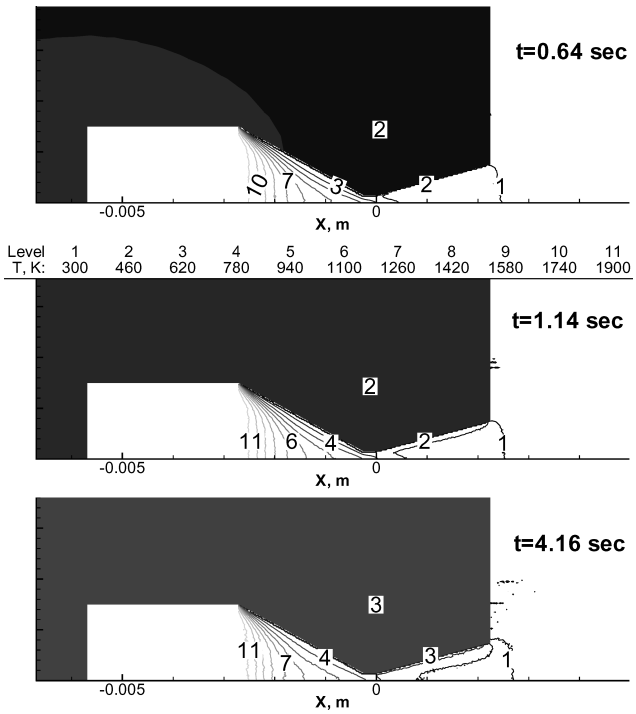

Fig. 11 Temperature field for case 5 in $Z = 0$ plane.

in Table 2. For all considered cases both thrust and mass-discharge coefficient decrease in time with increasing material temperature.

The mass-discharge coefficient decreases in time because of the increase of the thermal boundary layer as the wall temperature increases. The density in the thermal boundary layer is decreased as well as the flow velocity and thus the mass flow is diminished. A similar influence of the thermal wall boundary conditions on mass discharge was obtained in Ref. 18 for higher Reynolds numbers from 2×10^3 to 20×10^3.

The thrust of the micronozzle decreases with time much more significantly than in the two-dimensional case[7] due to higher viscous and heat transfer losses. For the lower stagnation pressure, $p_0 = 0.1$ atm, the final thrust values are 15% and 6% smaller than the initial values for cases 1 and 2, respectively. The corresponding decrease of the thrust in the two-dimensional case is only 2–3%.

The large temporal variation of the thrust and especially the mass-discharge coefficient in such microthrusters predicted by these simulations means that the coupling between gas flow and material thermal response has to be taken into account in micropropulsion system design.

VI. Conclusions

Gas-flow solutions as well as material thermal response for a microthruster at the throat-based Reynolds numbers of 35 and 175 were obtained using the direct simulation Monte Carlo method coupled to a finite element solution of the transient heat-transfer problem. Effects of the Reynolds number, thermal boundary conditions, and three-dimensional microthruster height on the flow structure and performance characteristics were considered.

The higher Reynolds number flow inside the micronozzle results in larger surface heat fluxes and, thus, it takes a shorter time for the material to reach its melting point. However, the heat fluxes and the operational time limits do not vary proportionally with the pressure due to a higher heat-flux coefficient at larger Knudsen numbers.

The cooling applied at the outer surface of the microthruster can sustain the thruster material temperature at a level which is lower than the melting temperature. Hence, the cooling allows for a longer thruster burn time. For both Reynolds numbers considered here the cooling results in improved nozzle performance in terms of higher mass discharge and thrust as a function of time.

The propulsive efficiency of both two- and three-dimensional micronozzle models decreases in time as the viscous losses increase for increasing wall temperatures. The large temporal variation of the thrust and especially the mass-discharge coefficient in such microthrusters is predicted by these simulations. Hence, the coupling between gas flow and material thermal response must be taken into account in micropropulsion system design.

Acknowledgment

The work performed at Penn State was supported by NASA John H. Glenn Research Center, under Grant NAG3-2590, technically monitored by Brian D. Reed. We thank Clifton Phillips of SPAWARSYSCEN, who provided us with computer time on the Department of Defense Maui High Performance Computing Center.

References

[1]Reed, B. D., de Groot, W., and Dang, L., "Experimental Evaluation of Cold Flow Micronozzles," AIAA Paper 2001-3521, July 2001.

[2]Bayt, R. L., and Breuer, K. S., "Viscous Effects in Supersonic MEMS-fabricated Nozzles," *Proceedings of the 3rd ASME Microfluidic Symposium*, Anaheim, CA, Nov. 1998.

[3]Hitt, D. L., Zakrzwski, C. M., and Thomas, M. A., "MEMS-Based Satellite Micropropulsion via Catalyzed Hydrogen Peroxide Decomposition," *Smart Materials and Structures*, Vol. 10, No. 6, 2001, pp. 1163–1175.

[4]Mueller, J., Chakraborty, I., Bame, D., and Tang, W., "Vaporizing Liquid Microthruster Concept—Preliminary Results of Initial Feasibility Studies," *Micropropulsion for Small Spacecraft*, edited by M. Micci and A. Ketsdever, Vol. 187, Progress in Astronautics and Aeronautics, AIAA, Reston, VA, 2000, pp. 215–230.

[5]London, A. P., Epstein, A. H., and Kerrebrock, J. L., "High-Pressure Bipropellant Microrocket Engine," *Journal of Propulsion and Power*, Vol. 17, No. 4, 2001, pp. 780–787.

[6]Alexeenko, A. A., Levin, D. A., Gimelshein, S. F., Collins, R. J., and Markelov, G. N., "Numerical Simulation of High-Temperature Gas Flows in a Millimeter-Scale Thruster," *Journal of Thermophysics and Heat Transfer*, Vol. 16, No. 1, 2002, pp. 10–16.

[7]Alexeenko, A. A., Fedosov, D. A., Gimelshein, S. F., Levin, D. A., and Collins, R. J., "Transient Heat Transfer and Gas Flow in a MEMS-Based Thruster," *IEEE Journal of Microelectromechanical Systems* (submitted for publication).

[8]Reed, B. D., "Decomposing Solid Micropropulsion Nozzle Performance Issues," AIAA Paper 2003-0672, Jan. 2003.

[9]De Groot, W. A., Reed, B. D., and Brenizer, M., "Preliminary Results of Solid Gas Generator Micropropulsion," AIAA Paper 98-3225, July 1998.

[10]Alexeenko, A. A., Levin, D., Gimelshein, S., Collins, R., and Reed, B., "Numerical Modeling of Axisymmetric and Three-Dimensional Flows in MEMS Nozzles," *AIAA Journal*, Vol. 40, No. 5, 2002, pp. 897–904.

[11]Reddy, J. N., and Gartling, D. K., *The Finite Element Method in Heat Transfer and Fluid Dynamics*, CRC Press, Boca Raton, FL, 2001.

[12]*Gridgen User Manual*, Pointwise, Inc., 1999.

[13]Bird, G. A., *Molecular Gas Dynamics and the Direct Simulation of Gas Flows*, Clarendon, Oxford, 1994.

[14]Ivanov, M. S., Markelov, G. N., and Gimelshein, S. F., "Statistical Simulation of Reactive Rarefied Flows: Numerical Approach and Applications," AIAA Paper 98-2669, June 1998.

[15]Incropera, F. P., and DeWitt, D. P., *Fundamentals of Heat and Mass Transfer*, Wiley, New York, 2001.

[16]Kandlikar, S. G., and Steike, M. E., "Predicting Heat Transfer During Flow Boiling in Minichannels and Microchannels," *ASHRAE Transactions*, Vol. 109, No. 1, 2003.

[17]Ivanov, M. S., and Gimelshein, S. F., "Current Status and Prospects of the DSMC Modeling of Near-Continuum Flows of Non-Reacting and Reacting Gases," *Rarefied Gas Dynamics*, AIP Conf. Proceedings, Vol. 663, 2003, pp. 339–348.

[18]Johnson, A. N., Espina, P. I., Mattingly, G. E., Wright, G. D., and Merkle, C. L., "Numerical Characterization of the Discharge Coefficient in Critical Nozzles," *Proceedings of the 1998 NCSL Workshop and Symposium*, Albuquerque, NM, 1998.